4-26-2021

Reconstructing primary production in a changing estuary: A mass balance modeling approach

Jongsun Kim

Mark J. Brush

Bongkeun Song

Iris C. Anderson

Reconstructing primary production in a changing estuary: a mass balance modeling approach

Jongsun Kim [a, *, 1], Mark J. Brush [a], Bongkeun Song [a], and Iris C. Anderson [a]

[a] Virginia Institute of Marine Science, William & Mary, Gloucester Point, VA

23062, USA.

*Corresponding author: jongsun@vims.edu

[1] Now at Graduate School of Oceanography, University of Rhode Island.

Running head: Primary production in a temperate estuary

Submitted to <u>Limnology and Oceanography</u>

ABSTRACT

Estuarine primary production (PP) is a critical rate process for understanding ecosystem function and response to environmental change. PP is fundamentally linked to estuarine eutrophication, and as such should respond to ongoing efforts to reduce nutrient inputs to estuaries globally. However, concurrent changes including warming, altered hydrology, reduced input of sediments, and emergence of harmful algal blooms (HABs) could interact with nutrient management to produce unexpected changes in PP. Despite its fundamental importance, estuarine PP is rarely measured. We reconstructed PP in the York River Estuary with a novel mass balance model based on dissolved inorganic nitrogen (DIN) for the period 1994-2018. Modeled PP compared well to previous estimates and demonstrated a long-term increase and down-estuary shift over the study period. This increase occurred despite reductions in discharge, flushing time, DIN loading, and DIN standing stock over the same period. Increased PP corresponded to increased water temperature, decreased turbidity and light attenuation, and increased photic depth and assimilation ratio, suggesting that phytoplankton in the York River Estuary have become more efficient at converting nutrients into biomass primarily due to a release from light limitation. The increase in PP also coincided with the increasing occurrence of late summer HABs in the lower York River Estuary, including the emergence of a second bloom-forming dinoflagellate in 2007. Results demonstrate how changes concurrent with nutrient management could alter expected system responses and illustrate the utility of the mass balance approach for estimating critical rate processes like PP in the absence of observations.

2

1. Introduction

Estuaries are among the most productive ecosystems in the world and provide numerous ecologically and economically important goods and services (Barbier et al. 2011; Costanza et al. 1997; Cloern 2014). Estuarine primary production (PP) generally provides the major input of organic carbon that fuels the food web in these systems, and is therefore a critical rate process for understanding system function, provision of ecosystem services, and response to environmental change. PP is also fundamentally linked to estuarine eutrophication, defined by Nixon (1995) as an increase in the rate of supply of organic matter (either autochthonous or allochthonous) to an ecosystem. Eutrophication causes numerous deleterious consequences in estuaries, including excessive accumulation of phytoplankton biomass, harmful (often toxic) algal blooms (HABs), reduced light penetration, loss of seagrasses, hypoxia/anoxia, and loss of fisheries (Brush et al. 2021; Cloern 2001; Kemp et al. 2005).

Estuarine PP is commonly controlled by nutrient availability, especially nitrogen (N), because most temperate coastal marine ecosystems are N-limited (Howarth and Marino, 2006; Nixon, 1986; Paerl, 2009). Rates of estuarine PP are often strongly correlated to nitrogen loading both within and across systems (Boynton et al. 1995; Nixon et al. 1996; Mallin et al. 1993). Accordingly, management efforts to reduce estuarine eutrophication have relied mainly on reduction of nitrogen loads, resulting in numerous improvements including reduced nutrient and chlorophyll-a concentrations, increased light penetration and concentrations of dissolved oxygen, and expanded seagrass habitat (Boesch, 2019; Lefcheck et al. 2018; Oviatt et al. 2017).

Despite the direct link between nutrient loading and estuarine PP, rates of productivity are also influenced by additional factors including climate change, the hydrologic cycle, and emergence of HABs. Climate change has the potential to impact the effectiveness of future

3

nutrient management actions due to increases in water temperature, changes in discharge, and increased frequency and intensity of storms (Najjar et al. 2010; Paerl and Huisman, 2008; Paerl et al. 2014).   For example, temperature increases associated with climate change will likely require greater nutrient load reductions to meet established dissolved oxygen criteria relative to reductions required under current temperatures (Lake and Brush, 2015b; Irby et al. 2018).   Changes in discharge affect not only nutrient loading but strength of stratification and estuarine flushing time, which affects the retention of phytoplankton and their ability to bloom (Paerl and Huisman, 2008; Lucas et al. 2009; Peierls et al. 2012).   While occurrence and spread of HABs have often been attributed to increased nutrient loading, they can be caused by several additional factors including warming, marine heatwaves, oxygen depletion, and changes to the hydrologic cycle (Anderson et al. 2002; Glibert and Burford, 2017; Gobler, 2020); whatever their cause, HABs represent large accumulations of photosynthetically-active biomass, and are thus likely to increase overall rates of estuarine PP (e.g., Song et al. 2009).

The Chesapeake Bay is an anthropogenically-enriched estuary where nutrient management has been ongoing for the last few decades with some success (Boesch 2019; Brush et al. 2021; Kemp et al. 2005).   As of 2016, loads of total nitrogen and phosphorus from watershed-based sources (both point and non-point) have been reduced by ~32% and ~40% relative to 1985 levels, respectively (Boesch, 2019; Brush et al. 2021), and this has translated into limited improvements in water quality (e.g., reduced surface nitrate and bottom hypoxia) and seagrass coverage (Murphy et al. 2011; Lefcheck et al. 2018; Harding et al. 2019).   However, chlorophyll-a concentrations have yet to decline (Harding et al. 2019; Brush et al. 2021), which may indicate that PP is also largely unchanged.   While ongoing nutrient load reductions are expected to result in a continued reversal of eutrophication, i.e., oligotrophication, this response could be altered due to interactions

4

with other stressors including warming water temperatures, altered hydrology, and ocean acidification (Brush et al. 2021). Najjar et al. (2010) summarized climate scenarios for the Chesapeake region, and reported projected increases in atmospheric CO_2 concentration, sea level, and water temperature of 50-160%, 0.7-1.6 m, and 2-6°C by 2100, respectively. While precipitation projections are more variable for the region, rates are expected to increase overall, especially in winter-spring, as is precipitation intensity, which will impact nutrient delivery, stratification, and flushing time.

The York River Estuary is a tributary of the Chesapeake Bay that has been subject to a similar history of nutrient loading, deteriorating water quality, and resulting efforts to reduce loads (Brush et al. 2021; Lake and Brush 2015a; Reay 2009). Total nitrogen and phosphorus loads to the York River Estuary have decreased by approximately one-third from their highest levels in the late 1990s, but chlorophyll-a concentrations have actually increased slightly while oxygen concentrations and Secchi depths are unchanged (Brush et al. 2021). This lack of response may be due at least in part to the strong influence of advective and tidal inputs across the mouth of the estuary from the mainstem Chesapeake Bay (Lake and Brush, 2015a, b). The lower York River Estuary has also been subject to increasing occurrences of HABs in recent decades; blooms of the dinoflagellate *Margalefidinium polykrikoides* have occurred since the 1960s (Marshall and Egerton, 2009; Mulholland et al. 2018; Zubkoff et al. 1979), and blooms of the dinoflagellate *Alexandrium monilatum* have occurred in most summers since 2007 (Reece, 2015).

Given the fundamental importance of PP in estuarine ecosystems and its central role in nutrient response and eutrophication, time series of estuarine PP are critical for understanding how these systems are changing due to nutrient management, climate change, and emergence of HABs. However, time series of estuarine PP are rare as monitoring programs usually only include

5

chlorophyll-a as a proxy of phytoplankton biomass (Nixon 2009). The only long-term time series

of PP in the Chesapeake Bay are Harding et al.'s (2002) measurements of ^{14}C water-column

integrated production for the mainstem (1982-2000), which does not cover the tributaries. The

only PP estimates for the major tributaries including the York River Estuary are the Chesapeake

Bay Program's (CBP) observations of light-saturated, maximum hourly productivity (P_{max}, 1984-

2009), but these do not reflect water-column integrated, daily PP. Additionally, neither dataset

spans the most recent decade(s) when responses to nutrient reductions and a changing climate are

likely to be accelerating. Thus, in this study, we applied a novel mass balance model based on

dissolved inorganic nitrogen (DIN) to reconstruct estuarine PP in the York River Estuary over a

25-year (1994-2018) time period to assess how this fundamental rate has changed in response to

nutrient management, climate change, and the emergence of late summer HABs. Mass balance

models are useful tools for calculating nutrient and carbon fluxes, estimating PP in coastal systems

from more readily measured variables, and providing insights into the biological and physical

mechanisms driving observed time series (Boyle et al. 1974; Kim et al. 2020a).

2. Data and Methods

2.1. Study area and data sources

The York River Estuary, a sub-estuary of the Chesapeake Bay in Virginia, is a relatively

shallow, mesotrophic, and microtidal system (Figure 1). It is a partially mixed estuary with a tidal

range of 0.5 to 1 m; average and maximum water depths are 5.1 and 25.7 m, respectively.

Depending on the season and year, the carbon (C) and nitrogen (N) cycles in this estuary are

regulated by numerous biological and physical drivers. For this study, we used the segmentation

of Lake and Brush (2015a, b), who split the York River Estuary into eight boxes along its axis

6

(Figure 1). These boxes were based on the long-term water quality monitoring stations of the U.S. Environmental Protection Agency's Chesapeake Bay Program (CBP). The York River Estuary receives riverine input from the Mattaponi and Pamunkey Rivers, which enter boxes 1 and 2, respectively, and from small streams along its entire length. Boxes 6 to 8, located in the lower York River Estuary, are regions vulnerable to intense late summer HABs (Figure 1).

Nutrient data for the York River Estuary were collected from the CBP (https://www.chesapeakebay.net) covering the period from 1994 through 2018. We conducted quality control and quality assurance (QC/QA) to remove inconsistencies and anomalies in the data for dissolved inorganic nitrogen (DIN) concentration, defined as the sum of ammonium (NH_4), nitrite (NO_2), and nitrate (NO_3) (e.g., removing outliers, missing data interpolations). Concentrations at each station were linearly interpolated between sampling dates to obtain a continuous record over the period of study. River discharge rates from each river were collected from USGS monitoring stations (Pamunkey: USGS 01673000 and Mattaponi: USGS 01674500) and scaled up to account for watershed area below the gauges (Lake and Brush 2015).

2.2. N-mass balance model

The DIN mass balance box model used in this study consists of a series of DIN input and output terms, and is modified from previous models to calculate the net removal of DIN inside each box, which when converted to carbon units represents potential primary production (PPP) (De Boer et al. 2010; Kim et al. 2020a) (Equation 1):

$$F_{Atmo}^{DIN} + F_{River}^{DIN} + F_{Bott}^{DIN} - F_{Dnf}^{DIN} - F_{Export}^{DIN} = F_{Removal}^{DIN} \qquad \text{Eq. 1}$$

7

where DIN concentration is the sum of ammonium, nitrate, and nitrite concentrations. All terms were specified in mol d^{-1} for each month from 1994 to 2018, and the model was solved monthly for $F_{Removal}^{DIN}$ (Table 1, Figure 2). F_{Atmo}^{DIN} is the flux from atmospheric nitrogen deposition (AN-D), which was obtained from the literature (0.3 mmol m^{-2} d^{-1}; Kemp et al. 2005; Lake and Brush, 2015a) and assumed to be equally distributed across all boxes. Total input to each box was computed by multiplying by the surface area of each box (A) using areas from Lake and Brush (2015a). F_{River}^{DIN} is the flux coming from riverine sources and was calculated from two factors $\left(C_{River}^{DIN} \times F_{River} \times 10^{-3}\right)$. C_{River}^{DIN} is the DIN concentration at CBP stations TF4.2 and TF4.4 upstream of Boxes 1 and 2, and F_{River} is the river discharge rate. The value of 10^{-3} converts from mmol to mol. F_{Bott}^{DIN} is the net benthic efflux of DIN from bottom sediments. Observational data are not available for the York River Estuary; thus, we used a value of 1.2 mmol N m^{-2} d^{-1} based on literature data for the lower Chesapeake Bay, scaled to the entire box using A (Cowan and Boynton, 1996; Boynton and Bailey, 2008). F_{Dnf}^{DIN} represents sedimentary denitrification rate; we applied a value of 78-108 µmol m^{-2} h^{-1} based on the literature (Kana et al. 2006). F_{Export}^{DIN} represents the loss of DIN from each box due to flushing and was calculated as the product of four terms: C_{EX}^{DIN} is the difference in DIN concentration between adjacent boxes, V_S is the water volume of each box (Lake and Brush 2015a), λ_{Flush} is the flushing rate of each box, computed as the reciprocal of flushing time, and 10^{-3} to convert from mmol to mol. Flushing times were computed as a function of riverine discharge using the freshwater fraction method (Officer 1980) within the model of Lake and Brush (2015a). Once all terms in equation 1 were specified, the model computed $F_{Removal}^{DIN}$ by difference, which represents net removal by biological production in each box of the York River Estuary.

As a mass balance box model, we assumed three factors; 1) the study area was in a steady state condition with balanced DIN inputs and outputs, 2) atmospheric deposition, benthic diffusion, and denitrification were evenly distributed across the York River Estuary, and 3) all remaining DIN was fully utilized by phytoplankton growth. Lake et al. (2013) estimated that phytoplankton contributed 95% of total organic carbon production during summer in the York River Estuary, so use of excess DIN by other primary producers appears minimal. Because we assumed that DIN was fully consumed by phytoplankton primary production, we calculated PPP in carbon units using the Redfield ratio (C: N: P = 106: 16: 1, molar). Since a large fraction of total dissolved nitrogen (TDN) in the York River Estuary occurs as dissolved organic nitrogen (DON), and some portion of that DON is likely bioavailable, the model was re-run using the observed time series of TDN to provide an upper estimate of PPP for comparison to PPP based on DIN alone.

3. Results

3.1. Validation of the Mass Balance Model

Since there are no available time series of PP in the York River Estuary, computed rates from the DIN mass balance model were compared to a limited dataset of summer (Jun-Sep 2008) phytoplankton primary production measured in the York River Estuary by Lake et al. (2013). Those rates were measured by constructing photosynthesis-irradiance curves from changes in oxygen in light-dark bottles, scaling over time and depth to obtain daily rates, and converting to carbon using an assumed photosynthetic quotient (mol O_2 : mol C) of 1.0 (Lake et al. 2013). Measured daily PP from Lake et al. (2013) was 2.22 g C m^{-2} d^{-1}, which was nearly identical to the average of 2.18 g C m^{-2} d^{-1} computed over the same time period with the DIN mass balance model (Figure 3). Modeled rates of PP were slightly higher than the observations in the lower estuary

9

(Boxes 6-8), and slightly lower in the middle estuary (Boxes 3-5). However, the small differences between modeled and measured PP, and the identical patterns along the axis of the estuary, demonstrate the mass balance model is estimating reasonable rates of PP in the York River Estuary. While the pattern of computed PPP using TDN was almost identical to that using DIN, the average rate in summer 2008 was 3.53 g C m^{-2} d^{-1}. This is a great deal higher than the average rate using the DIN mass balance model, as well as previous observations (Lake et al. 2013).

3.2. Reconstructed Primary Production in the York River Estuary

The model predicted a long-term increase in PPP in the York River Estuary, with most of the increase occurring in the mid-2000s (Figure 4). The model also predicted a change in the spatial distribution of PP in the York River Estuary. Early in the time series (before 2006), most of the modeled PP occurred in the upper half of the estuary (57%), but after 2006, a much greater percentage occurred in the lower estuary (68%) (Figure 4). Computed increases in PPP occurred in all months (Figure S1) and all regions of the York River Estuary (Figure S2).

The computed increase in PPP in the York River Estuary coincided with a long-term increase in surface chlorophyll-a concentrations based on CBP monitoring data, at least in the upper estuary (Figure 5a). The increase also corresponded with an increase in light-saturated, ^{14}C-based rates of P_{max} and associated assimilation ratios observed in the York River Estuary by the CBP, although the time series ended in early 2009 (Figures 5b-c). These observed increases in P_{max} occurred in all months and at stations in both the upper and lower York River Estuary (Figure S3), similar to modeled results (Figures S1, S2).

The modeled increase in PPP occurred despite long-term declines in riverine discharge, flushing time, and total standing stock of DIN in the York River Estuary (Figure 6a, b). The

10

combination of decreasing discharge and ongoing nutrient management also translated into decreasing DIN loads over this time period (Figure 6c). Export of DIN from the York River Estuary (between box 8 and Chesapeake Bay) was similarly predicted to have decreased over the study period, while biological removal of N ($F_{Removal}^{DIN}$) was predicted to increase markedly (Figure 6c).

Riverine loading was the dominant source of DIN to the York River Estuary both before and after 2006, with a small decline in importance in the latter period due to decreased discharge and ongoing nutrient management (Figure 7). This input was mostly balanced by biological uptake via primary production which dominated the outputs, with export making up most of the difference (Figure 7). The increase in productivity after 2006 resulted in a corresponding decrease in export.

4. Discussion

The mass balance approach produced rates of PPP that compared well with the limited observations of Lake et al. (2013) (Figure 3). Rates of computed PPP more closely matched prior estimates when using DIN (2.18 g C m^{-2} d^{-1}) rather than TDN (3.53 g C m^{-2} d^{-1}) in the mass balance model. Given this, we conclude that computed PPP using DIN is more accurate than that using TDN, which suggests a relatively small portion of DON in the York River Estuary is bioavailable. DON bioavailability in the York River Estuary has yet to be directly measured. However, some of the additional PPP computed using TDN may reflect uptake of DON via osmotrophy by dinoflagellates, which often dominate the phytoplankton community especially in summer (Mulholland et al. 2018; Reece, 2015). Osmotrophy can occur in the absence of light and, thus, would not contribute to PP based on the photosynthetic incubations used to calibrate the Lake and Brush (2015a) model.

11

The model estimated a long-term increase in PPP in the system occurring in all months and all regions of the estuary, with greatest increases in the mid-2000s in the lower estuary (Figures 4, S1, S2). This increase is supported by similar increases in light-saturated P_{max} which also occurred in all months and at both the head and mouth of the system and increases in chlorophyll-a at the head of the estuary (Figures 5a, b, S3). The predicted long-term increase in PPP also corresponds with the emergence of a second toxic dinoflagellate that produces intense summer blooms in the lower estuary, *A. monilatum*. However, the increase in PPP occurred despite overall reductions in discharge, flushing time, DIN loading, and DIN standing stock (Figure 6), and despite relatively constant chlorophyll-a concentrations in the lower estuary where most of the increase in PPP was computed to occur (Figure 5a).

4.1. What Explains the Increase in PPP?

Despite the long-term decreases in riverine discharge and DIN load over the study period, most of those declines occurred prior to 2006, while discharge and loads after 2006 were relatively stable with the exception of 2018 which was an unusually wet year (Figure 6a, c). The standing stock of DIN also became relatively stable after 2006 (Figure 6b). This change in the trends of discharge, load, and standing stock in the mid-2000s and greater stability after that time may have been at least partly responsible for the increase in computed PPP.

The increase in assimilation ratios (P_{max}:chlorophyll-a, Figure 5c) suggests that phytoplankton have become more efficient at converting DIN into biomass since the mid-2000s. We attribute this primarily to a release of light limitation owing to other long-term changes occurring in the York River Estuary over the study period. An analysis of the long-term CBP monitoring data indicate long-term warming of York River Estuary surface waters over the study

12

period (Figure 8a), which could be partly responsible for the increase in production given the well-established exponential relationship between temperature and phytoplankton growth (Eppley 1972; Brush et al. 2002). Probably more important is that turbidity has also decreased across the York River Estuary during the study period (Figure 8b), resulting in a long-term reduction in the vertical attenuation coefficient for light (k_D), most notably at the head of the system (Figure 8c). Most importantly, computed photic depths (Z_p, depth of 1% surface irradiance, $Z_p = 4.61/k_D$, Brush et al. 2002) have increased over the study period, particularly in the deeper, lower estuary where most of the volume occurs and most of the increase in computed PPP took place. The modeled increase in PPP despite reductions in DIN load and standing stock (and faster flushing of phytoplankton) is therefore most likely due to increased light penetration, deeper photic depths, and thus increased utilization of available DIN in the estuary. Interestingly, bottom water O_2 concentrations have exhibited a long-term decline over the study period (Figure 8d) which could be due in part to increased production, sinking, and microbial respiration of autochthonous organic matter, although it is likely more attributable to reduced solubility under warming temperatures.

The increase and down-estuary shift in modeled PP in the mid-2000s also coincided with the emergence of intense summer blooms of *A. monilatum* in the lower estuary (Reece 2015). As noted above, the lower Chesapeake Bay including the York River Estuary has been subject to increasing occurrences of HABs in recent decades. Blooms of *M. polykrikoides* have occurred since the 1960s (Marshall and Egerton, 2009; Mulholland et al. 2018; Zubkoff et al. 1979), and blooms of *A. monilatum* have occurred in most summers since 2007 (Reece, 2015). Many dinoflagellates, including *M. polykrikoides*, are capable of growth in the dark using osmotrophy (uptake of dissolved organic matter) (Mulholland et al. 2018), which may have contributed to the increase in PPP observed in recent years and down-estuary. Interestingly, less than 15% of PPP

13

was computed to occur in the lower York River Estuary in years when these HABs did not occur, compared to ~30-40% in bloom years (data not shown). While the cause of these HABs is not well understood, the computed increase in PPP since the mid-2000s may be at least partly attributable to their increasing occurrence, particularly the emergence of *A. monilatum* since 2007.

There may also have been other processes which we have not accounted for in the model, and more work is needed to identify the various biological and physical mechanisms controlling the increase in PPP in this system. Regardless, the computed increase in PPP suggests that despite long-term efforts to control eutrophication by reducing nutrient loads, the York River Estuary may actually have become more eutrophic since the mid-2000s due to changes in other variables such as temperature and turbidity, the latter also likely due to improved watershed management via reduced sediment loading. This highlights the challenge of managing nutrient-fueled eutrophication in a system undergoing other concurrent changes (e.g., climate, HABs, reduced sediment inputs; sensu Cloern 2001), that is connected to a much larger estuary (e.g., Lake and Brush 2015a), and subject to non-linear recovery trajectories (e.g., Duarte et al. 2009). It also suggests that additional reductions in loading may be necessary to meet established water quality criteria (e.g., Lake and Brush 2015b; Irby et al. 2018).

4.2. Role of Multiple Nutrient Sources

The mass balance modeling approach facilitates determination of the major and minor DIN inputs to the York River Estuary, and comparison to other systems where the approach has been applied. Both this study and the Lake and Brush (2015a) simulation modeling study of the York River Estuary found that riverine and diffuse watershed sources dominated the input of nitrogen, with less input from atmospheric deposition and benthic fluxes. Similarly, Kim et al. (2020a)

14

found that the significant input to the Gulf of Mexico was from rivers with minor contributions from atmospheric deposition and submarine groundwater discharge. Conversely, the coastal sea off Korea receives greater contributions from both atmospheric deposition and submarine groundwater discharge, which were important controlling factors of predicted PPP (Kim, 2018).

Similar to the previous mass balance study in the Gulf of Mexico (Kim et al. 2020a), there was a lack of observational data for both atmospheric deposition and benthic effluxes in the York River Estuary, so these represent two terms where additional data would help better constrain our budget. While these are currently relatively minor terms in the budget, they may become more important with continued watershed-based nutrient management or with changes in watershed discharge. However, atmospheric deposition is also expected to decrease over time as it is also the subject of management efforts aimed at reducing this source of nitrogen to the Chesapeake Bay (Boesch, 2019).

4.3. Utility of the Mass Balance Modeling Approach

Water quality and biogeochemical simulation models are widely used tools for understanding and predicting the dynamics of estuarine ecosystems (Brush and Harris 2016; Ganju et al. 2016). These models have been increasingly used to understand long-term ecosystem responses to changes in nutrient loading and co-occurring stressors such as climate change, and to inform management decisions aimed at improving water quality and restoring habitat. This includes several modeling studies in the Chesapeake Bay and its tributaries (e.g., Cerco and Noel, 2004; Lake and Brush, 2015a; Testa et al. 2014). These models are mathematical simplifications of real ecosystems that combine detailed mechanistic formulations to simulate system-level processes including nitrogen cycling and PP through space and time. They span a wide range of

both ecological and hydrodynamic complexity that reflects an ongoing trade-off between precision, realism, and generality (Levins 1966; Brush and Harris 2016; Ganju et al. 2016). These models often take substantial amounts of time to construct and run, and require large amounts of data for model development, calibration, and validation.

Mass balance models like the one developed here provide an alternate approach for constraining system-level processes through construction of material budgets for carbon, nutrients, or oxygen at larger spatial and temporal scales (e.g., Bierman et al. 1994; Kim 2018; Kim et al. 2020a). They are useful tools for calculating material fluxes and estimating system-wide processes including PP and net ecosystem metabolism in coastal systems (Kim et al. 2020a). A recent application of the approach in the Gulf of Mexico supported the delineation of productivity zones linked to nutrient-salinity ratios (Kim et al. 2020b). These models have been successfully applied in many systems, including the Patuxent River estuary of the Chesapeake Bay (Testa et al. 2008), the mainstem Chesapeake Bay (Testa et al. 2018), and around the world through the Land Ocean Interactions in the Coastal Zone (LOICZ) program (e.g., Ramesh et al. 2015; Smith et al. 2010; Swaney et al. 2011). These models tend to have fewer data requirements and can be developed and applied more quickly than mechanistic simulation models.

This study represents an application of the mass balance modeling approach to investigate long-term changes in primary production in the York River Estuary, a system undergoing nutrient management and a number of concurrent changes. The mass balance approach produced rates of PPP that compared well with a limited dataset of observed PP, and model predictions revealed a long-term increase and down-estuary shift in productivity despite ongoing reductions in nutrient loading. This analysis was made possible by the availability of long-term measurements of watershed discharge, nutrient loading, and estuarine concentrations of DIN and salinity (to

16

compute flushing times), but did not require the additional data and resources required for traditional model development, calibration, and validation. In the absence of a time series of direct measurements of PP in this system, the mass balance approach provided a novel means of reconstructing this vital rate for analysis in the context of long-term changes in the ecosystem. The analysis illustrates the utility of the mass balance approach for estimating PP in other estuarine systems, since this critical rate is typically not measured as part of traditional monitoring programs.

Author contributions

JK conceived and designed this study and conducted the modeling. JK and MB analyzed

the results and wrote the manuscript. All co-authors provided input on the methods, assumptions,

and data sources, and all commented on the manuscript.

Acknowledgements

Conflict of Interest

None declared.

References

Anderson, D. M., Glibert, P. M., and Burkholder, J. M. 2002. Harmful algal blooms and eutrophication: Nutrient sources, composition, and consequences. Estuaries, 25, 704-726.

Barbier, E.B., Hacker, S.D., Kennedy, C., Koch, E.W., Stier, A.C., Silliman, B.R., 2011. The value of estuarine and coastal ecosystem services. Ecological Monographs 81, 169–193. doi:10.1890/10-1510.1

Bierman, V. J., Hinz, S. C., Wiseman, Jr. W. J., Rabalais, N. N., and Turner, R. E. 1994. A Preliminary Mass Balance Model of Primary Productivity and Dissolved Oxygen in the Mississippi River Plume/Inner Gulf Shelf Region. Estuaries., 17(4), 886-899.

Boesch, D. F. 2019. Barriers and bridges in abating coastal eutrophication. 2019. Front. Mar. Sci. 6, 23. doi: 10.3389/fmars.2019.00123

Boynton, W. R., Garber, J.H., Summers, R., and Kemp, W.M., 1995. Inputs, transformations, and transport of nitrogen and phosphorus in Chesapeake Bay and selected tributaries. Estuaries 18:285–314.

Boynton, W. R. and Bailey, E. M. 2008. Sediment oxygen and nutrient exchange measurements from Chesapeake Bay, tributary rivers, and Maryland coastal bays: development of a comprehensive database & analysis of factors controlling patterns and magnitude of sediment-water exchanges. University of Maryland, Center for Environmental Science Technical Report Series. TS-542-08.

Brush, M. J., Brawley, J. W., Nixon, S. W., and Kremer, J. N. 2002. Modeling phytoplankton production: Problems with the Eppley curve and an empirical alternative. Marine ecological progress series. 238:31-45.

Brush, M. J., and Harris, L. A. 2016. Ecological modeling. Pp. 214-223 in: Kennish, M.J. (ed.), Encyclopedia of Estuaries. Encyclopedia of Earth Sciences Series, Springer Netherlands.

Brush, M. J., M. Giani, C. Totti, J. Testa, J. Faganeli, N. Ogrinc, W.M. Kemp, and S. Fonda. 2021. Eutrophication, harmful algae, oxygen depletion, and acidification. Ch. 5 in: Malone, T.C., A. Malej, and J. Faganeli (eds.), Coastal Ecosystems in Transition: A Comparative Analysis of the Northern Adriatic and Chesapeake Bay. Geophysical Monograph 256, First Edition, American Geophysical Union. John Wiley & Sons, Inc.

Cerco, C. F., Noel, M. R. 2004. The 2002 Chesapeake Bay Eutrophication Model. Report EPA 903-R-04-004, Chesapeake Bay Program Office, U.S. Environmental Protection Agency, Annapolis, MD.

Costanza, R., d'Arge, R., Groot, R., Farber, S., Grasso, M., Hannon, B., Limburg, K., Naeem, S., O'Neill, R., Paruelo, J., Raskin, R, Sutton, P., and Belt, M. 1997. The value of the world's ecosystem services and natural capital. Nature. 387:253-260.
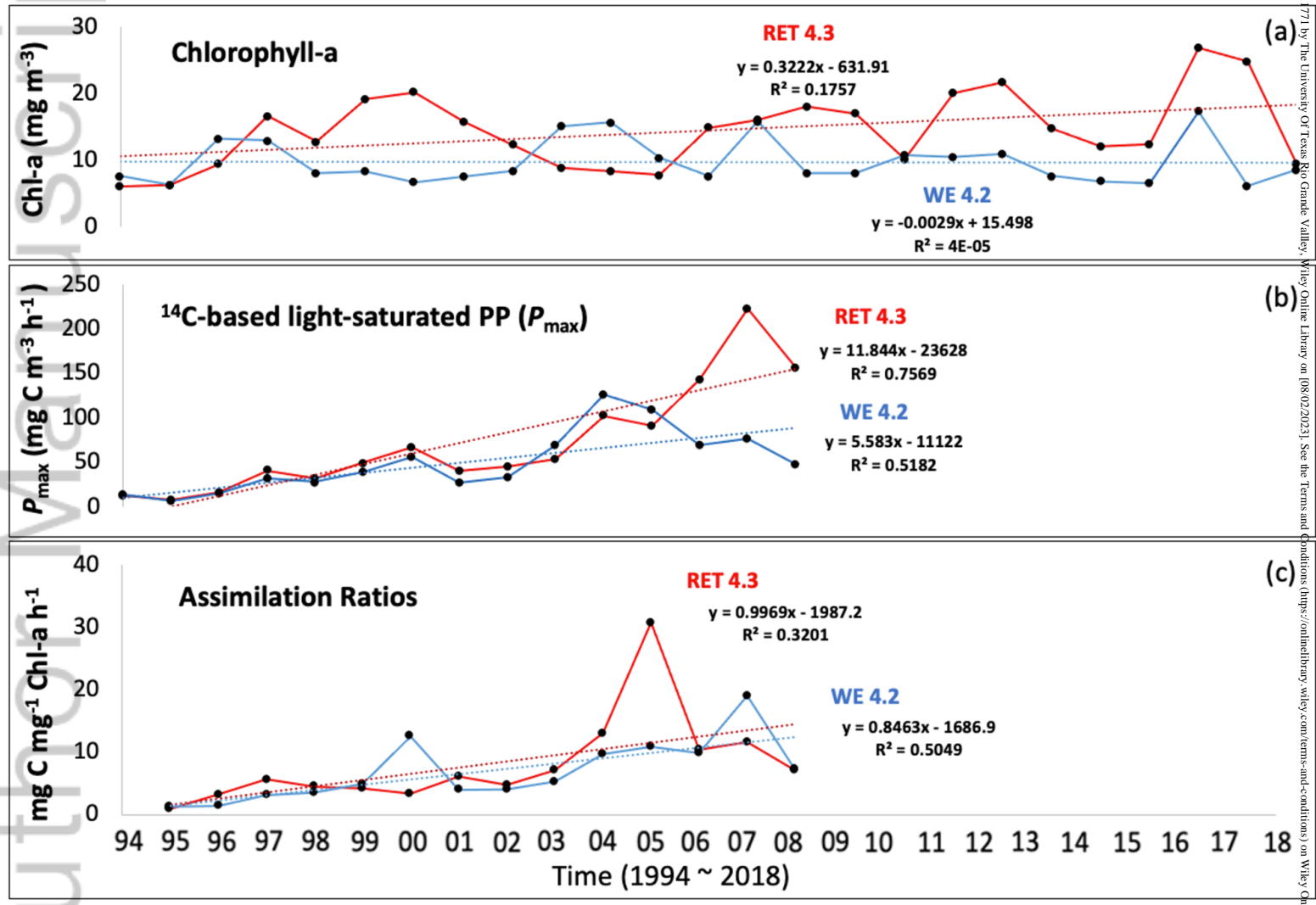
Cowan, J. L., and Boynton, W. R. 1996. Sediment-water oxygen and nutrient exchanges along the longitudinal axis of Chesapeake Bay: seasonal patterns, controlling factors and ecological significance. Estuaries 19: 562–580.

Cloern, J. E. 2001. Our evolving conceptual model of the coastal eutrophication problem, Mar. Ecol. Prog. Ser. 210, 223–253.

Cloern, J. E., Foster, S. Q., and Kleckner, A. E. 2014. Phytoplankton primary production in the world's estuarine-coastal ecosystem. Biogeosciences. 11, 2477-2501.

De Boer, A. M., Watson, A. J., Edwards, N. R., and Oliver, K. I. C. 2010. A multi-variable box model approach to the soft tissue carbon pump. Climate of the past. 6, 827-841.

Duarte, C. M., Conley, D. J., Carstensen, J., and Sánchez‐Camacho, M. 2009. Return to Neverland: Shifting baselines affect eutrophication restoration targets. Estuaries and Coasts, 32(1), 29–36.

Eppley, R. W. 1972. Temperature and phytoplankton growth in the sea. Fish. Bull. 70: 1063–1085.

Flint, R. W, Powell, G. L, and Kalke, R. D. 1986. Ecological effects from the balance between new and recycled nitrogen in Texas coastal water. Estuaries. 9(4A):284-294.

Ganju, N. K., Brush, M. J., Rashleigh, B., Aretxabaleta, A. L., del Barrio, P., Grear, J. S., Harris, L. A., Lake, S. J., McCardell, G., O'Donnell, J., Ralston, D. K., Signell, R. P., Testa, J. M., and Vaudrey J. M. P. 2016. Progress and challenges in coupled hydrodynamic-ecological estuarine modeling. Estuaries and Coasts 39:311–332.

Glibert, P. M., and Burford, M. A. 2017. Globally changing nutrient loads and harmful algal blooms: Recent advances, new paradigms, and continuing challenges. Oceanography 30(1):58–69, https://doi.org/10.5670/oceanog.2017.110.

Gobler, C. J. 2020. Climate change and harmful algal blooms: Insights and perspective. Harmful Algae, 91, 101731, doi.org/10.1016/j.hal.2019.101731.

Greening, H., and Janicki, A. 2006. Toward reversal of eutrophic conditions in a subtropical estuary: water quality and seagrass response to nitrogen loading reductions in Tampa Bay, Florida, USA. Environmental Management, 38(2), 163-178.

Harding, Jr., L. W., Mallonee, M. E., and Perry, E. S. 2002. Toward a predictive understanding of primary productivity in a temperate, partially stratified estuary. Estuarine, Coastal and Shelf Science, 55(3), 437-463.

Harding, Jr., L. W., Mallonee, M. E., Perry, E. S., Miller, W. D., Adolf, J. E., Gallegos, C. L., and Paerl H. W. 2019. Long-term trends, current status, and transitions of water quality in Chesapeake Bay. Scientific Reports, 9, 6709-6728.

Howarth, R. W., and Marion, R. 2006. Nitrogen as the limiting nutrient for eutrophication in coastal marine ecosystems: Evolving views over three decades. Limnology and Oceanography., 51, 364-376.

Irby, I. D., Friedrichs, M. A. M., Friedrichs, C. T., Bever, A., Hood, R. R., Lanerolle, L. W. J., Li, M., Linker, L., Scully, M., Sellner, K., Shen, J., Testa, J., Wang, H., Wang, P., and Xia, M. 2016. Biogeosciences 13(7): 2011–2028.

Kana, T. M., Cornwell, J. C., and Zhong, L. 2006. Determination of denitrification in the Chesapeake Bay from measurements of N2 accumulation in bottom water. Estuaries and Coasts 29: 222–231.

Kemp, W. M., Boynton, W.R., Adolf, J.E., Boesch, D.F., Boicourt, W.C., Brush, G., Cornwell, J.C., Fisher, T.R., Glibert, P.M., Hagy, J.D., Harding, L.W., Houde, E.D., Kimmel, D.G., Miller, W.D., Newell, R.I.E., Roman, M.R., Smith, E.M., and Stevenson, J.C. 2005. Eutrophication of Chesapeake Bay: historical trends and ecological interactions. Marine Ecology Progressive Series 303: 1–29.

Kim, J. S. 2018. Implications of different nitrogen input sources for primary production and carbon flux estimates in coastal waters. Texas A&M University. Ph.D. Dissertation.

Kim, J. S., Chapman, P., Rowe, G. T. DiMarco, S. F., and Thornton, D. C. O. 2020a. Implications of different nitrogen input sources for potential production and carbon flux estimates in the coastal Gulf of Mexico (GOM) and Korean Peninsula coastal waters. Ocean Science, 16, 45–63.

Kim, J. S., Chapman, P., Rowe, G. T., and DiMarco, S. F. 2020b. Categorizing zonal productivity on the continental shelf with Nutrient-Salinity ratios. Journal of Marine Systems, 206, 103336

Lake, S. J., Brush, M. J., Anderson, I. C., and Kator, H. I. 2013. Internal versus external drivers of periodic hypoxia in a coastal plain tributary estuary: the York River, Virginia. Marine Ecological Progressive Series 492: 21–39.

Lake, S. J., and Brush, M. J. 2015a. Contribution of Nutrient and Organic Matter Sources to the Development of Periodic Hypoxia in a Tributary Estuary. Estuaries and Coasts 38:2149-2171.

Lake, S. J., and Brush, M. J. 2015b. Modeling estuarine response to load reductions in a warmer climate: York River Estuary, Virginia, USA, Mar. Ecol. Prog. Ser., 538, 81–98, https://doi.org/10.3354/meps11448.

Lefcheck, J. S., Orth, R. J., Dennison, W. C., Wilcox, D. J., Murphy, R. R., Keisman, J., Gurbisz, C., Hannam, M., Landry, J. B., Moore, K. A., Patrick, C. J., Testa, J., Weller, D. E., and Batiuk, R. A. 2018. Long-term nutrient reductions lead to the unprecedented recovery of a
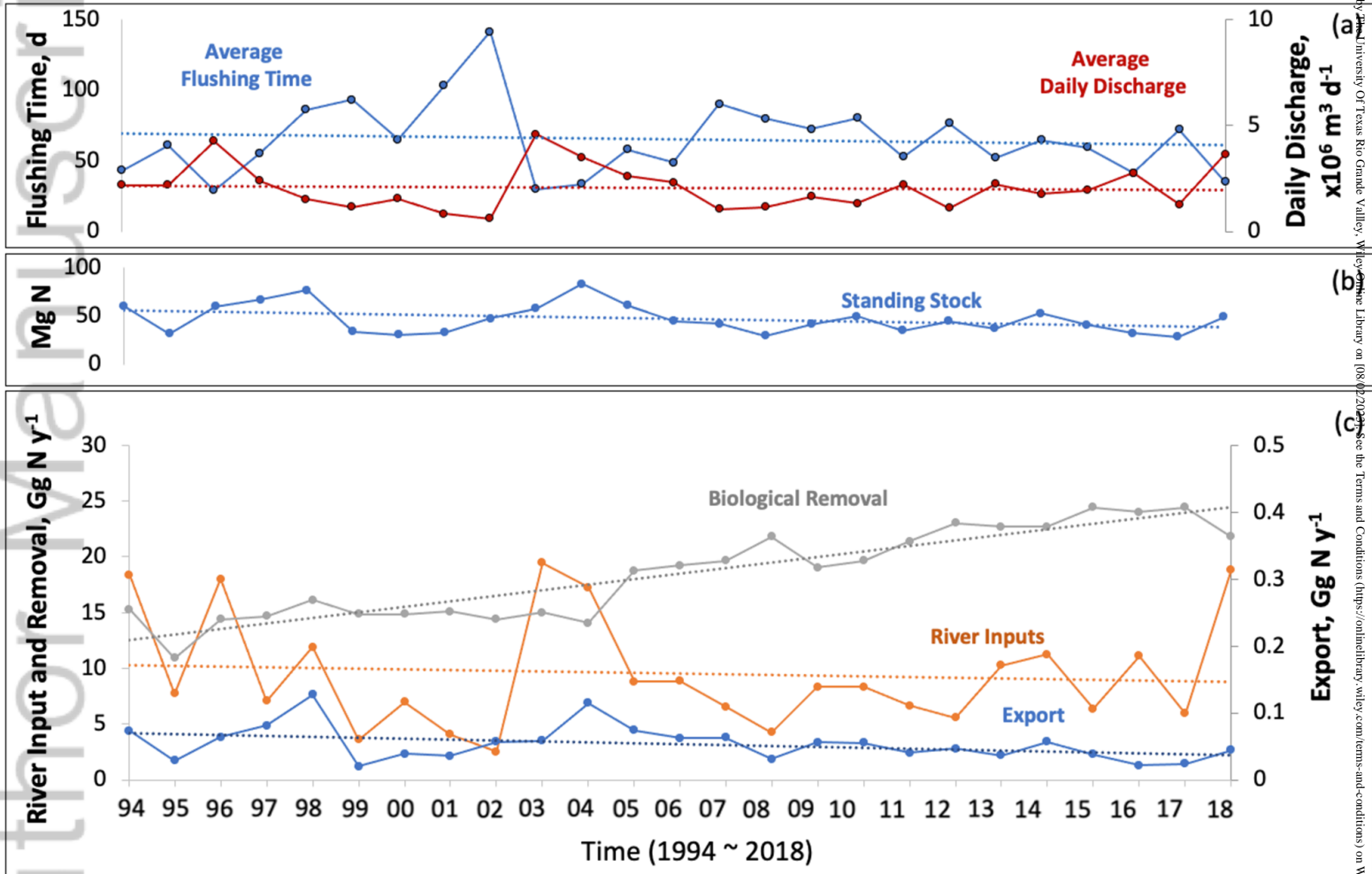
21

temperate coastal region. Proceedings of the National Academy of Science, 115(14), 3658-3662.

Levins, R. 1966. The strategy of model building in population biology. American Scientist, 54, 421-431.

Lin, J., and Kuo, A.Y. 2003. A Model Study of Turbidity Maxima in the York River Estuary, Virginia. Estuaries, 26, 1269-1280.

Lucas, L. V., Thompson, J. K., and Brown, L. R. 2009. Why are diverse relationships observed between phytoplankton biomass and transport time? Limnology and Oceanography, 54, 381-390.

Murphy, R. R., Kemp, W. M, and Ball. W. P. 2011. Long-term trends in Chesapeake Bay seasonal hypoxia, stratification, and nutrient loading. Estuaries and Coasts, 34(6), 1293-1309.

Najjar, R. G., Pyke, C. R., Adams, M. B., Breitburg, D., Hershner, C., Kemp, M., Howarth, R., Mulholland, M. R., Paolisso, M., Secor, D., Sellner, K., Wardrop, D., and Wood, R. 2010. Potential climate-change impacts on the Chesapeake Bay. Estuarine, Coastal and Shelf Scinece, 86, 1-20.

Nixon, S.W. 1986. Nutrient dynamics and the productivity of marine coastal waters. In Marine environment and pollution, ed. R. Halwagy, D. Clayton, and M. Behbehani, 97–115. Oxford: The Alden Press.

Nixon, S. W. 1995. Coastal marine eutrophication: a definition, social causes, and future concerns. Ophelia 41:199–219.

Nixon, S. W., Ammerman, J. M., Atkinson, L. P., Berounsky, V. M., Billen, G., Boicourt, W. C., Boynton, W. R., Church, T. M., Ditoro, D. M., Elmgren, R., Garber, J. H., Giblin, A. E., Jahnke, R. A., Owens, N. J. P., Pilson, M. E. Q., and Seitzinger, S. P. 1996. The fate of nitrogen and phosphorus at the land-sea margin of the North Atlantic Ocean. Biogeochemistry, 35: 141-180.

Mallin, M. A., Pearl, H.W., Rudek, J., and Bates, P.W., 1993. Regulation of estuarine primary production by watershed rainfall and river flow. Marine Ecology Progress Series 93:199–203.

Marshall, H. G., and Egerton, T. A. 2009. Phytoplankton blooms: Their occurrence and composition within Virginia's tidal tributaries. Virginia Journal of Science, 60(3), 149–164.

Mulholland, M., Morse, R., Boneillo, G., Bernhardt, P., Filippino, K., Procise, L., . . . Gobler, C. 2009. Understanding Causes and Impacts of the Dinoflagellate, Cochlodinium polykrikoides, Blooms in the Chesapeake Bay. Estuaries and Coasts, 32(4), 734-747.

Mulholland, M. R., Morse, R., Egerton, T., Bernhardt, P. W., and Filippino, K. C. 2018. Blooms of dinoflagellate mixotrophs in a lower Chesapeake Bay tributary: Carbon and nitrogen uptake over diurnal, seasonal, and interannual timescales. Estuaries and Coasts, 41(6), 1744–1765.

Officer, C.B. 1980. Box models revisited. In Estuarine and wetland processes with emphasis on modeling, ed. P. Hamilton and K.B. MacDonald, 65–114. New York: Plenum Press.

Oviatt, C., Smith, L., Krumholz, J., Coupland, C., Stoffel, H., Keller, A., McManus, M.C., and Reed, L. 2017. Managed nutrient reduction impacts on nutrient concentrations, water clarity, primary production, and hypoxia in a north temperate estuary. Estuarine, Coastal and Shelf Science, 199, 25-34.

Paerl, H. W., and J. Huisman. 2008. Blooms like it hot. Science. 320: 57–58.

Paerl, H. W. 2009. Controlling Eutrophication along the Freshwater-Marine Continuum: Dual Nutrient (N and P) Reductions are Essential. Estuaries and Coasts., 32, 593-601.

Paerl, H. W., Hall, N. S., Peierls, B. L., and Rossignol, K. L. 2014. Evolving paradigms and challenges in estuarine and coastal eutrophication dynamics in a culturally and climatically stressed world. Estuar. Coasts 37, 243–258. doi: 10.1007/s12237-014-9773-x

Peierls, B. L., Hall, N. S., and Paerl, H. W. 2012. Non-monotonic responses of phytoplankton biomass accumulation to hydrologic variability: A comparison of two coastal plain North Carolina estuaries. Estuaries and Coasts, 35, 1376-1392.

Ramesh. R., Chen. Z., Cummins. V., Day. J., D'Elia. C., Dennison. B., Forbes. D. L., Glaeser. B., Claser. M., Clavovic. B., Kremer. H., Lange. M., Larsen. J. N., Tissier. M. Le., Newton. A., Pelling. M., Purvaja. R., and Wolanski. E. 2015. Land-ocean interactions in the coastal zone: past, present & future, Anthtropocene., 12, 85-98.

Reay, W. G. 2009. Water quality within the York River Estuary. Journal of Coastal Research. S1. 57. 23-39.

Reece, K.S. 2015. Monitoring for HAB species in VA waters of Chesapeake Bay during 2015: Emerging HAB species in Chesapeake Bay (Annual report #VIMSHAB617FY16). Richmond, VA: Virginia Department of Health.

Song, X., Huang, L., Zhang, J., Huang, H., Li, T., and Su, Q. 2009. Harmful algal blooms (HABs) in Daya Bay, China: An in-situ study of primary production and environmental impacts. Marine Pollution Bulletin, 58, 1310-1318.

Testa, J. M., Kemp, W. M., Boynton, W. R., and Hagy, J. D. 2008. Long-term changes in water quality and productivity in the Patuxent river estuary: 1985 to 2003. Estuaries and Coasts., 31, 1021-1037.

Testa, J. M., Li, Y., Lee, Y. J., Li, M., Brady, D. C., Di Toro, D. M., Kemp, W. M., and Fitzpatrick, J. J. 2014. Quantifying the effects of nutrient loading on dissolved O2 cycling and hypoxia in Chesapeake Bay using a coupled hydrodynamic–biogeochemical model. Journal of Marine Systems 139: 139–158.

Testa, J. M., Kemp, W. M., & Boynton, W. R. 2018. Season-specific trends and linkages of nitrogen and oxygen cycles in Chesapeake Bay: Linked oxygen and nitrogen trends. Limnology and Oceanography, 63(5), 2045–2064.

Smith, S. V., Swaney, D. P., and Talaue-McManus, L. 2010. Carbon–Nitrogen–Phosphorus Fluxes in the Coastal Zone: The LOICZ Approach to Global Assessment. In: Liu KK., Atkinson L., Quiñones R., Talaue-McManus L. (eds) Carbon and Nutrient Fluxes in Continental Margins. Global Change – The IGBP Series. Springer, Berlin, Heidelberg

Swaney, D. P., Smith, S. V., and Wulff, F. 2011. The LOICZ biogeochemical modeling protocol and its application to estuarine ecosystems. Pp. 135-159 in: Wolanski, E., and McLusky, D. (eds.), Treatise on Estuarine and Coastal Science v. 9, Estuarine and Coastal Ecosystem Modelling. Academic Press, London.

Zubkoff, P.L., Munday, J.C., Rhodes, R.G., & Warriner, J.E. 1979. Mesoscale features of summer (1975 to 1977) dinoflagellate blooms in the York River, Virginia (Chesapeake Bay estuary). In F.J.R. Taylor, H.H. Seliger (Eds.), Toxic Dinoflagellate Blooms, Proceedings of the 2nd International Conference on Toxic Dinoflagellate Blooms (pp. 279–286). New York: Elsevier North Holland.
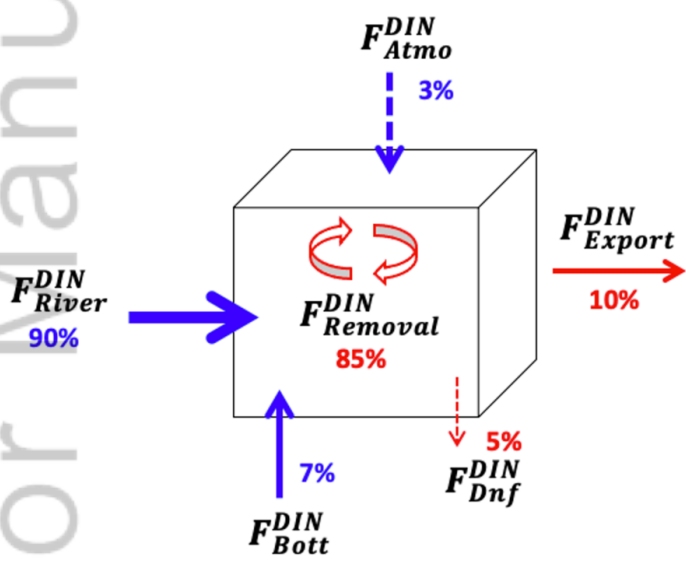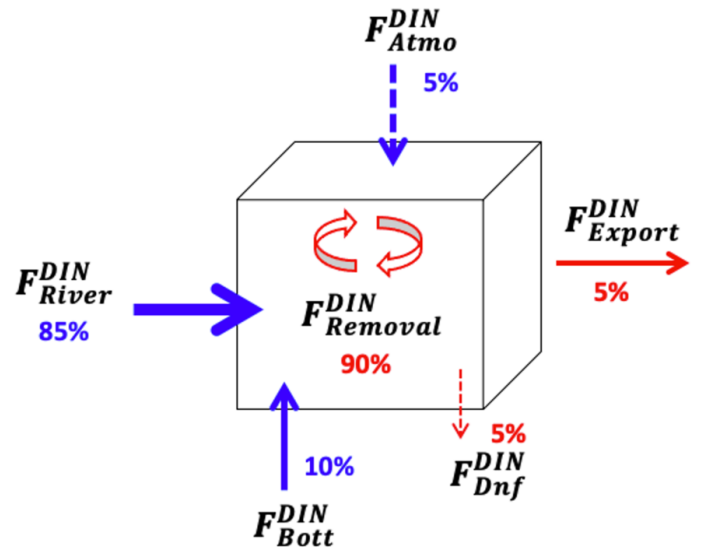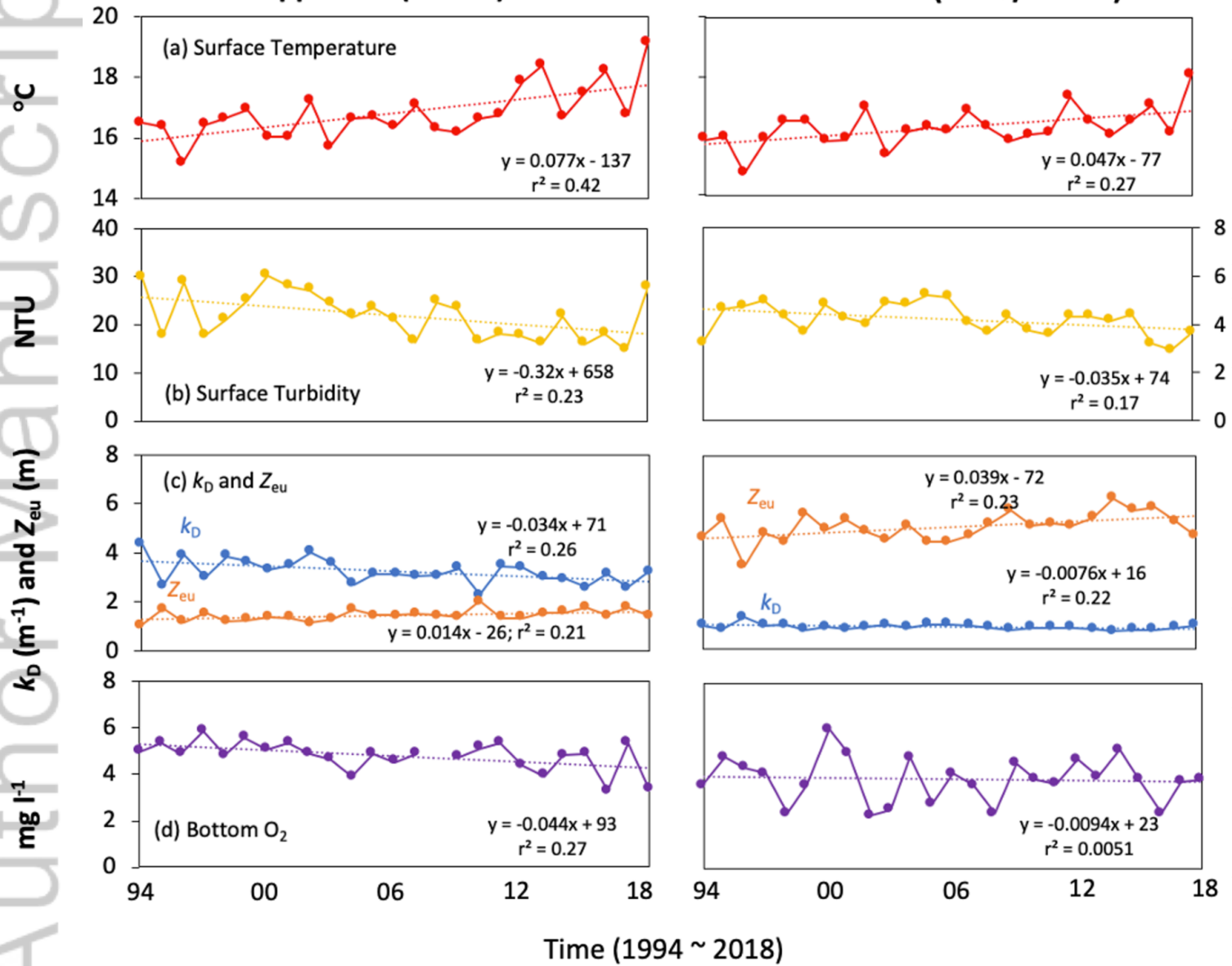
LNO_11771_fig5.png

LNO_11771_fig6.png

(a) 1994-2006

F^{DIN}_{Atmo} 3%

F^{DIN}_{Export} 10%

F^{DIN}_{River} 90%

$F^{DIN}_{Removal}$ 85%

F^{DIN}_{Dnf} 5%

F^{DIN}_{Bott} 7%

(b) 2006-2018

F^{DIN}_{Atmo} 5%

F^{DIN}_{Export} 5%

F^{DIN}_{River} 85%

$F^{DIN}_{Removal}$ 90%

F^{DIN}_{Dnf} 5%

F^{DIN}_{Bott} 10%

LNO_11771_fig7.png

Upper YRE (RET4.3)

Lower YRE (LE4.3/WE4.2)
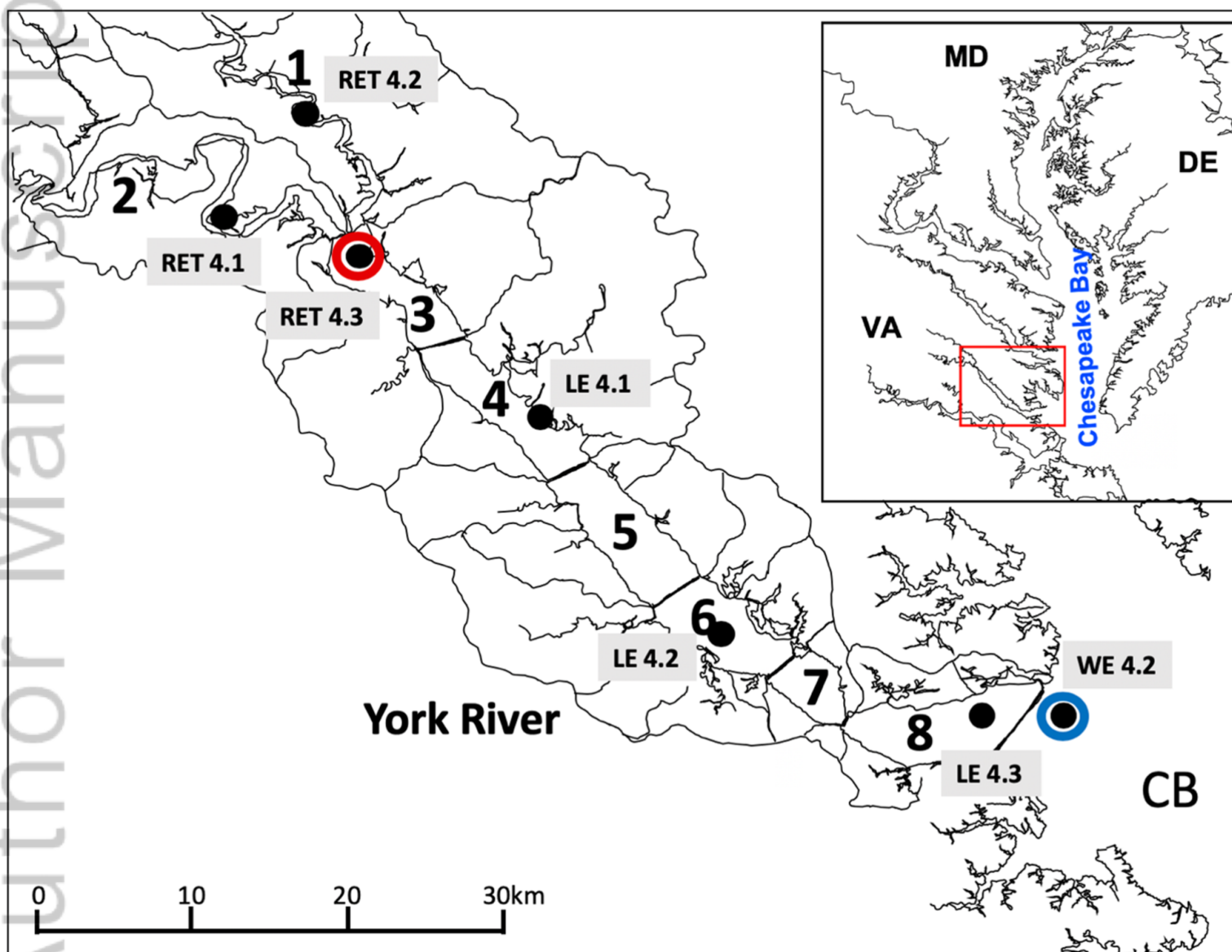
(a) Surface Temperature

$y = 0.077x - 137$
$r^2 = 0.42$

$y = 0.047x - 77$
$r^2 = 0.27$

(b) Surface Turbidity

$y = -0.32x + 658$
$r^2 = 0.23$

$y = -0.035x + 74$
$r^2 = 0.17$

(c) k_D and Z_{eu}

k_D

Z_{eu}

$y = -0.034x + 71$
$r^2 = 0.26$

$y = 0.014x - 26; r^2 = 0.21$

$y = 0.039x - 72$
$r^2 = 0.23$

Z_{eu}

k_D

$y = -0.0076x + 16$
$r^2 = 0.22$

(d) Bottom O_2

$y = -0.044x + 93$
$r^2 = 0.27$

$y = -0.0094x + 23$
$r^2 = 0.0051$

Time (1994 ~ 2018)
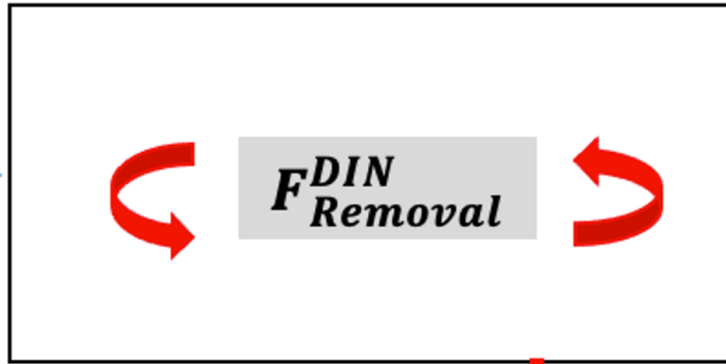
LNO_11771_fig8.png

LNO_11771_Fig.1.png
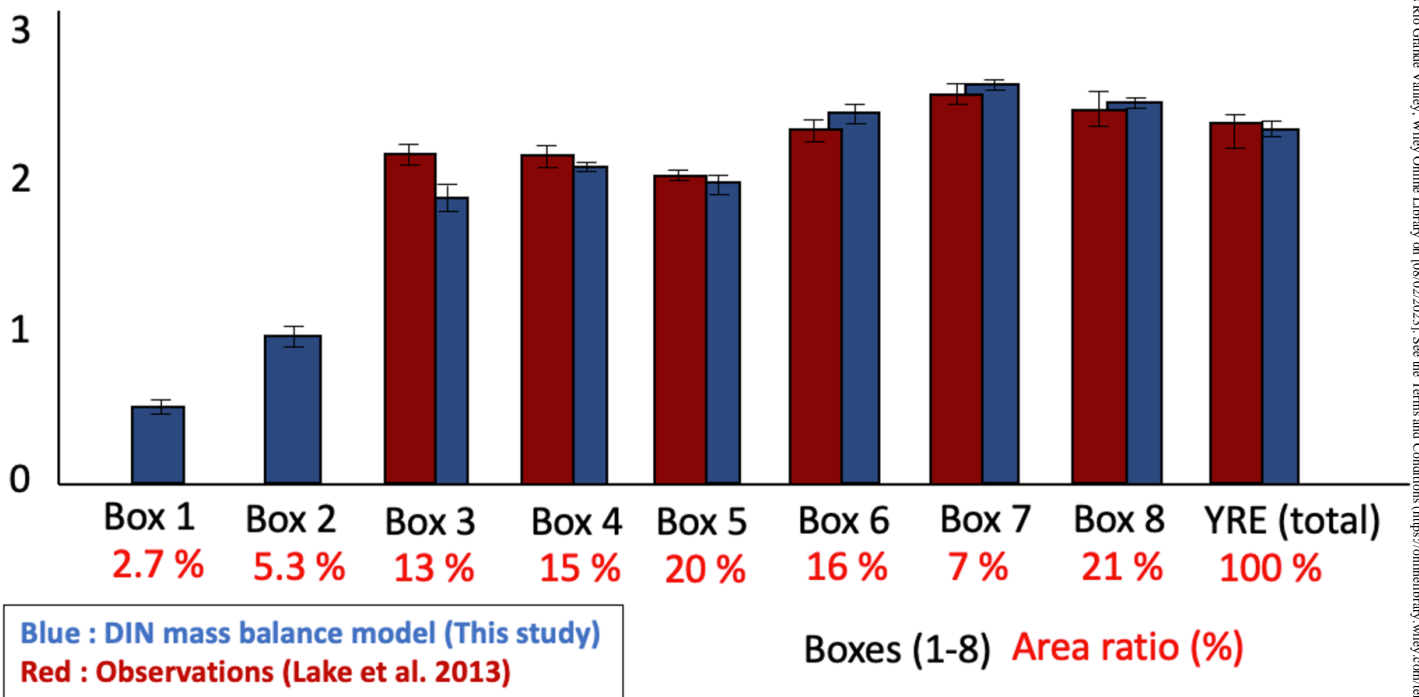
LNO_11771_Fig.2.png

LNO_11771_Fig.3.png
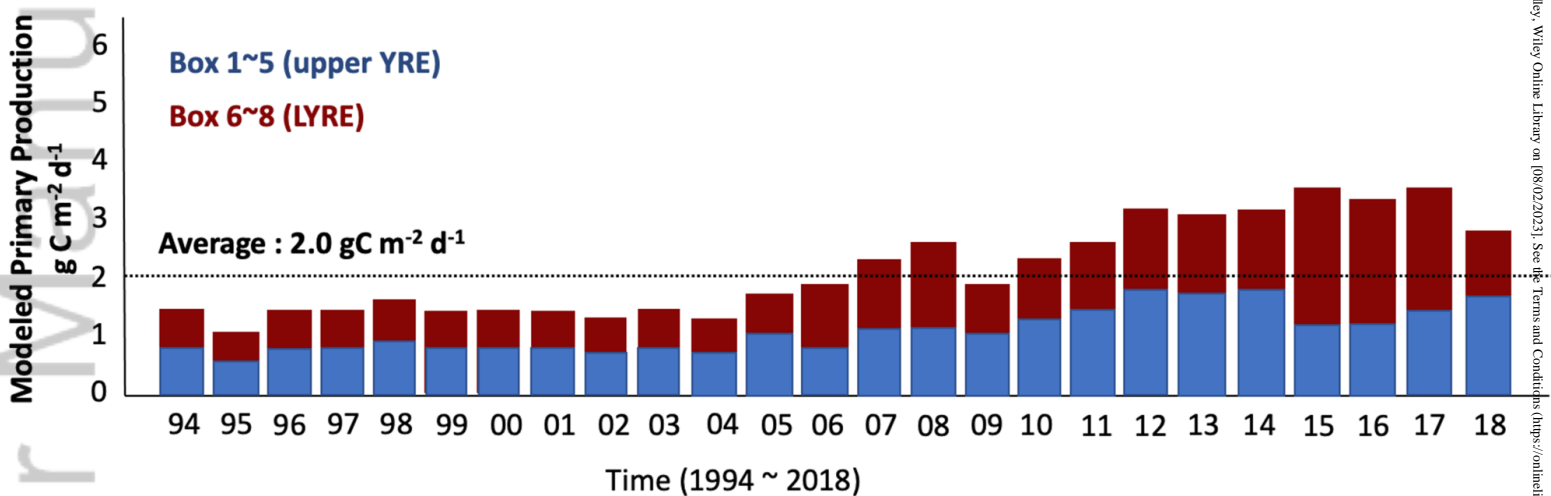
LNO_11771_Fig.4.png

List of Figures

Figure 1. Map of the York River Estuary (YRE) and the Chesapeake Bay. Numbered segments show the boxes from Lake and Brush (2015 a, b) that were used in the current box model application. Boxes 1 and 2 receive input from the Mattaponi and Pamunkey Rivers, respectively, which are the major sources of DIN to the YRE. Points show the locations of CBP monitoring stations used in this analysis; red and blue circles show the locations of the chlorophyll-a and ^{14}C primary productivity data.

Figure 2. Inputs (blue) and outputs (red) of DIN (see text for details) in the York River Estuary (YRE) mass balance model, following the approach of Kim et al. (2020). Fluxes represent river inputs (F_{River}), atmospheric deposition (F_{Atmo}), flushing (F_{Export}), denitrification (F_{Dnf}), sediment effluxes (F_{Bott}), and net uptake to support primary production ($F_{Removal}$). The model assumes steady state conditions; all fluxes are computed in mol d^{-1}.

Figure 3. Comparison of mean summer (Jun-Sep) primary production estimated from the mass balance model to observed rates from Lake et al. (2013). Both modeled and observed rates are from 2008. Lake et al. (2013) did not make measurements in Boxes 1-2. Rates for YRE (total) are based on Boxes 3-8 only. Percentages in red indicate the percent of total YRE area in each box. Error bars represent one standard deviation.

Figure 4. Predicted primary production from the mass balance model from 1994 to 2018. Values are expressed as the average daily rate each year and are broken out by region of the YRE.

Figure 5. Time series of (a) surface chlorophyll-a, (b) ^{14}C-based, light-saturated primary productivity (P_{max}), and (c) assimilation ratios from CBP monitoring stations RET4.3 and WE4.2 in the upper and lower YRE, respectively. The primary production monitoring program ended in September 2009.

Figure 6. (a) Flushing time and daily discharge, (b) standing stock of DIN, and (c) computed DIN fluxes for the entire YRE. Linear regression equations for DIN standing stock (y = -0.71x + 1471; r^2 = 0.12), river inputs (y = -0.064x + 137; r^2 = 0.01), biological removal (y = 0.50x – 983; r^2 = 0.85), and export (y = -0.001x + 2.8; r^2 = 0.15) as a function of year were all highly significant (p < 0.0001).

Figure 7. Annual DIN budgets for the YRE from the mass balance model, (a) averaged over the period 1994 to 2006 and (b) 2006 to 2018. Values are expressed as the percent contribution to total inputs (blue terms) and total outputs (red terms).

Figure 8. Time series of annual average (a) surface water temperature, (b) surface turbidity, (c) vertical attenuation coefficient (k_D) and euphotic depth (Z_{eu}), and (d) bottom oxygen concentration (averaged below the pycnocline) from CBP monitoring stations in the upper and lower YRE, respectively (see Fig. 1).
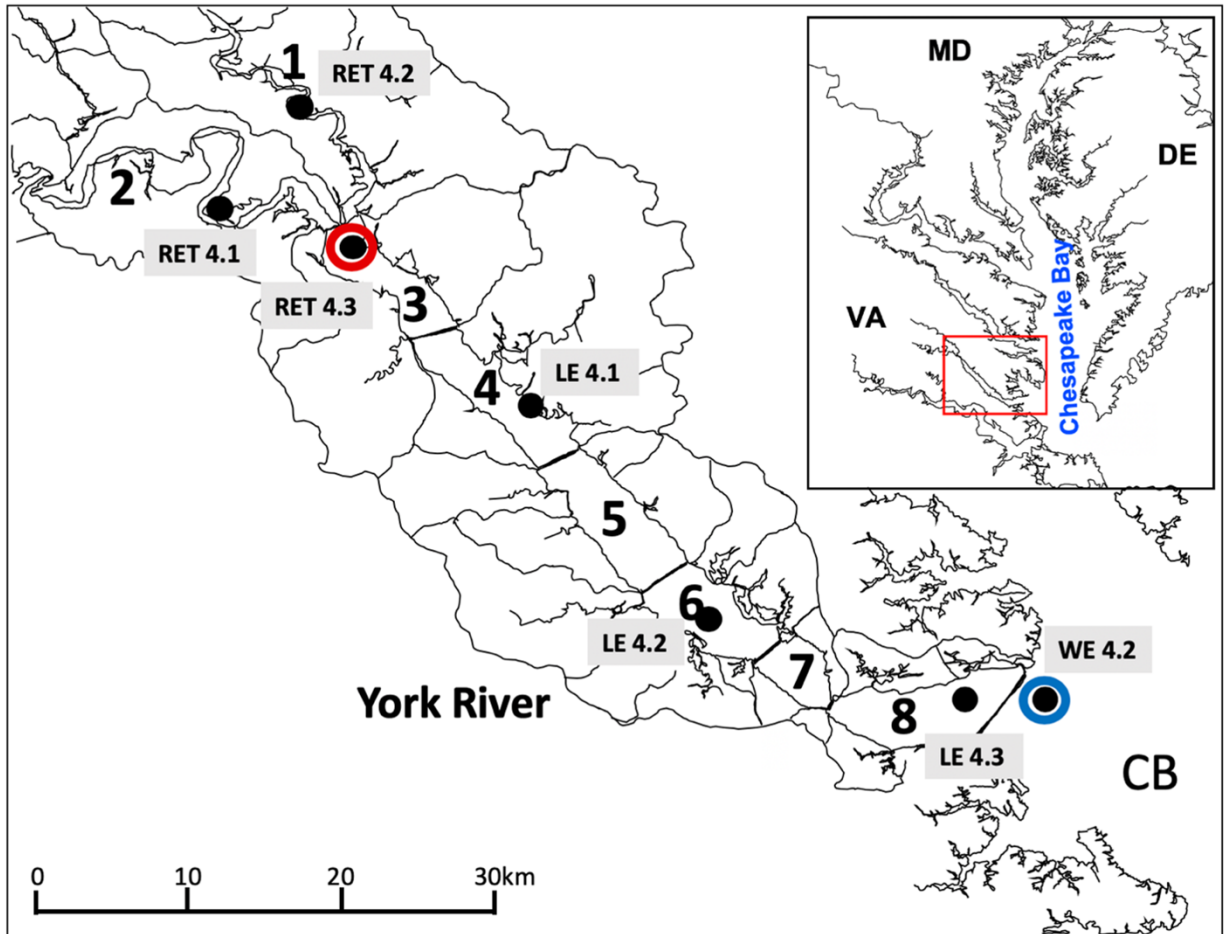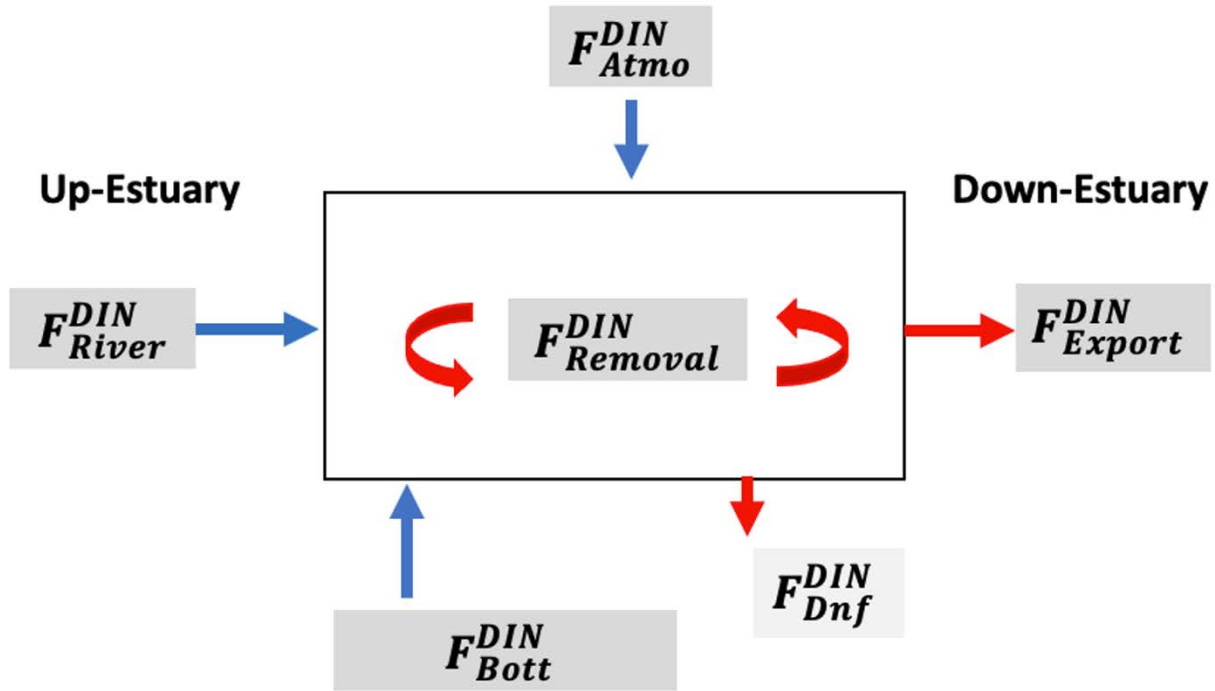
1

Figure 1. Map of the York River Estuary (YRE) and the Chesapeake Bay. Numbered segments show the boxes from Lake and Brush (2015 a, b) that were used in the current box model application. Boxes 1 and 2 receive input from the Mattaponi and Pamunkey Rivers, respectively, which are the major sources of DIN to the YRE. Points show the locations of CBP monitoring stations used in this analysis; red and blue circles show the locations of the chlorophyll-a and ^{14}C primary productivity data.

Figure 2. Inputs (blue) and outputs (red) of DIN (see text for details) in the York River Estuary (YRE) mass balance model, following the approach of Kim et al. (2020). Fluxes represent river inputs (F_{River}), atmospheric deposition (F_{Atmo}), flushing (F_{Export}), denitrification (F_{Dnf}), sediment effluxes (F_{Bott}), and net uptake to support primary production ($F_{Removal}$). The model assumes steady state conditions; all fluxes are computed in mol d^{-1}.
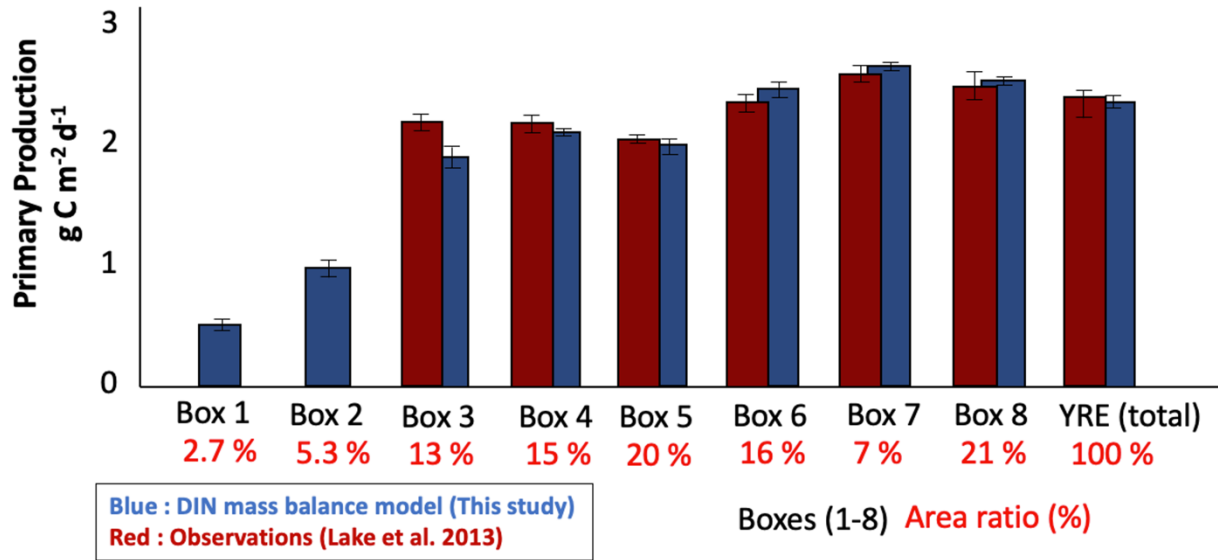
3

Figure 3. Comparison of mean summer (Jun-Sep) primary production estimated from the mass balance model to observed rates from Lake et al. (2013). Both modeled and observed rates are from 2008. Lake et al. (2013) did not make measurements in Boxes 1-2. Rates for YRE (total) are based on Boxes 3-8 only. Percentages in red indicate the percent of total YRE area in each box. Error bars represent one standard deviation.
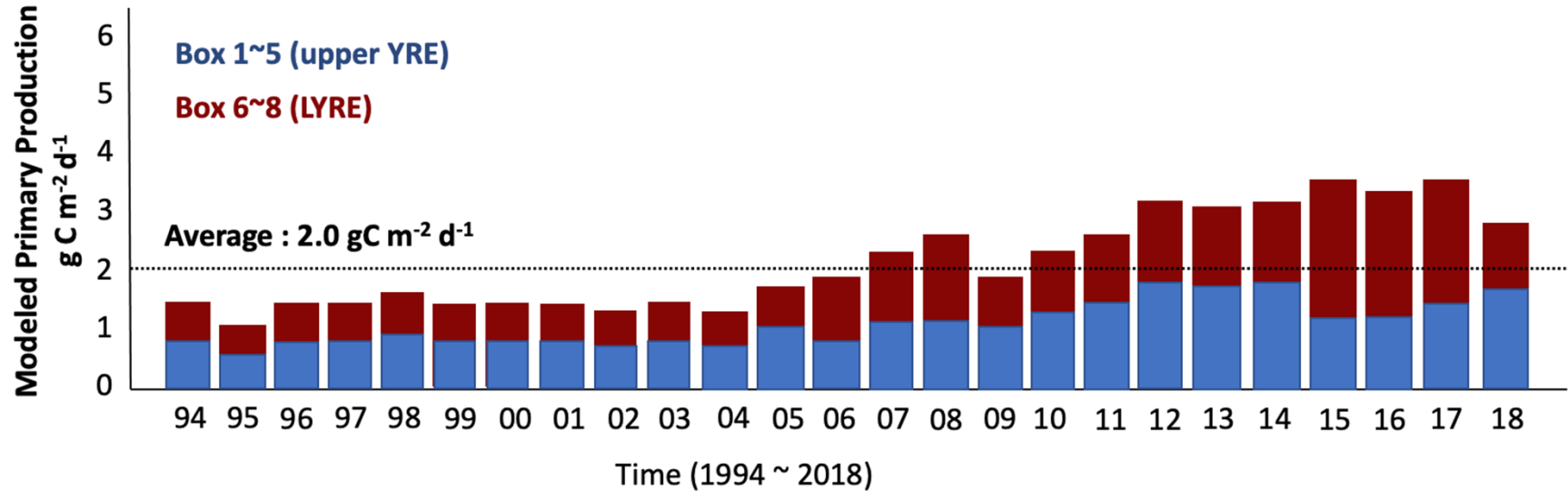
Figure 4. Predicted primary production from the mass balance model from 1994 to 2018. Values are expressed as the average daily rate each year and are broken out by region of the YRE.
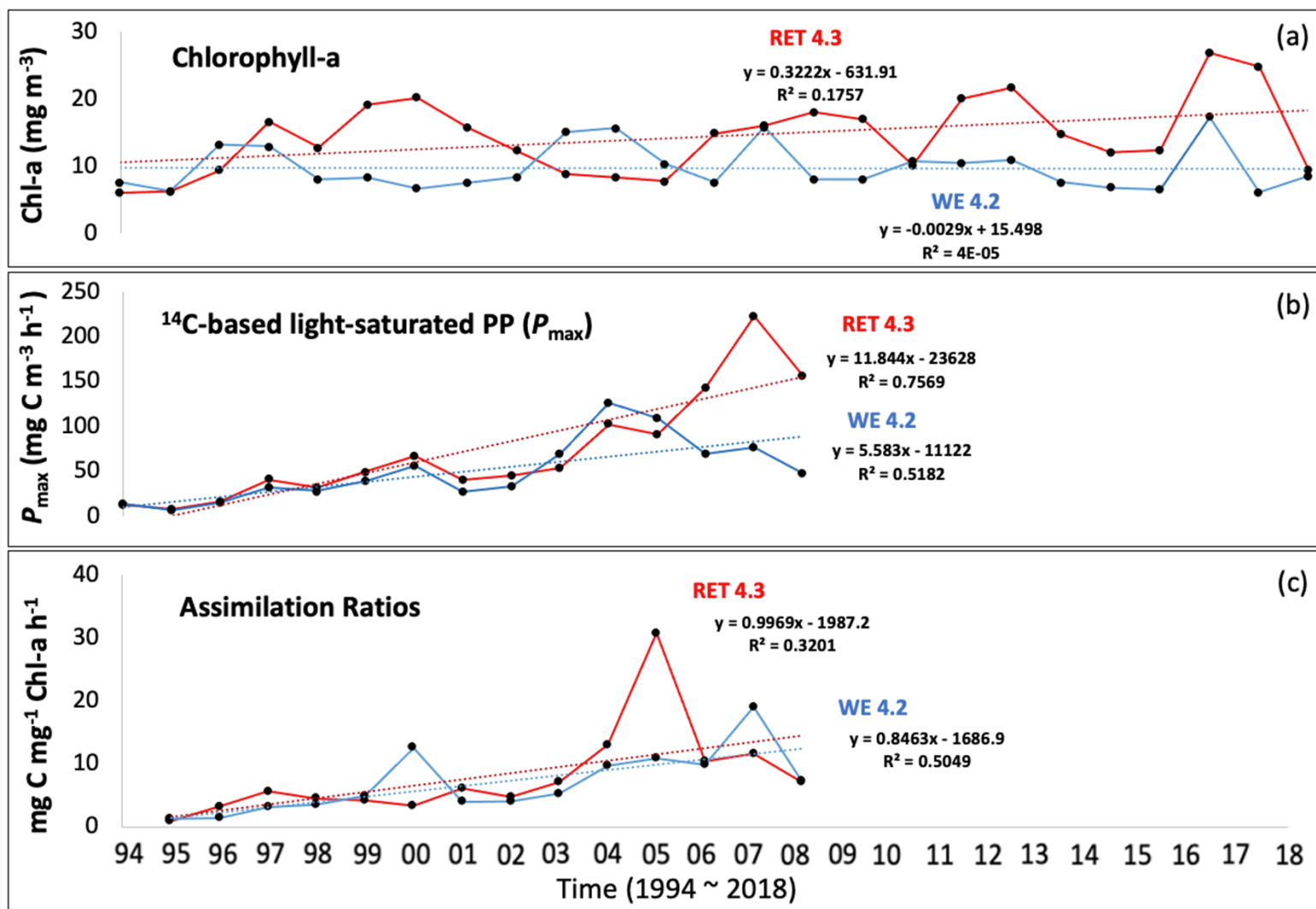
Figure 5. Time series of (a) surface chlorophyll-a, (b) ^{14}C-based, light-saturated primary productivity (P_{max}), and (c) assimilation ratios from CBP monitoring stations RET4.3 and WE4.2 in the upper and lower YRE, respectively. The primary production monitoring program ended in September 2009.
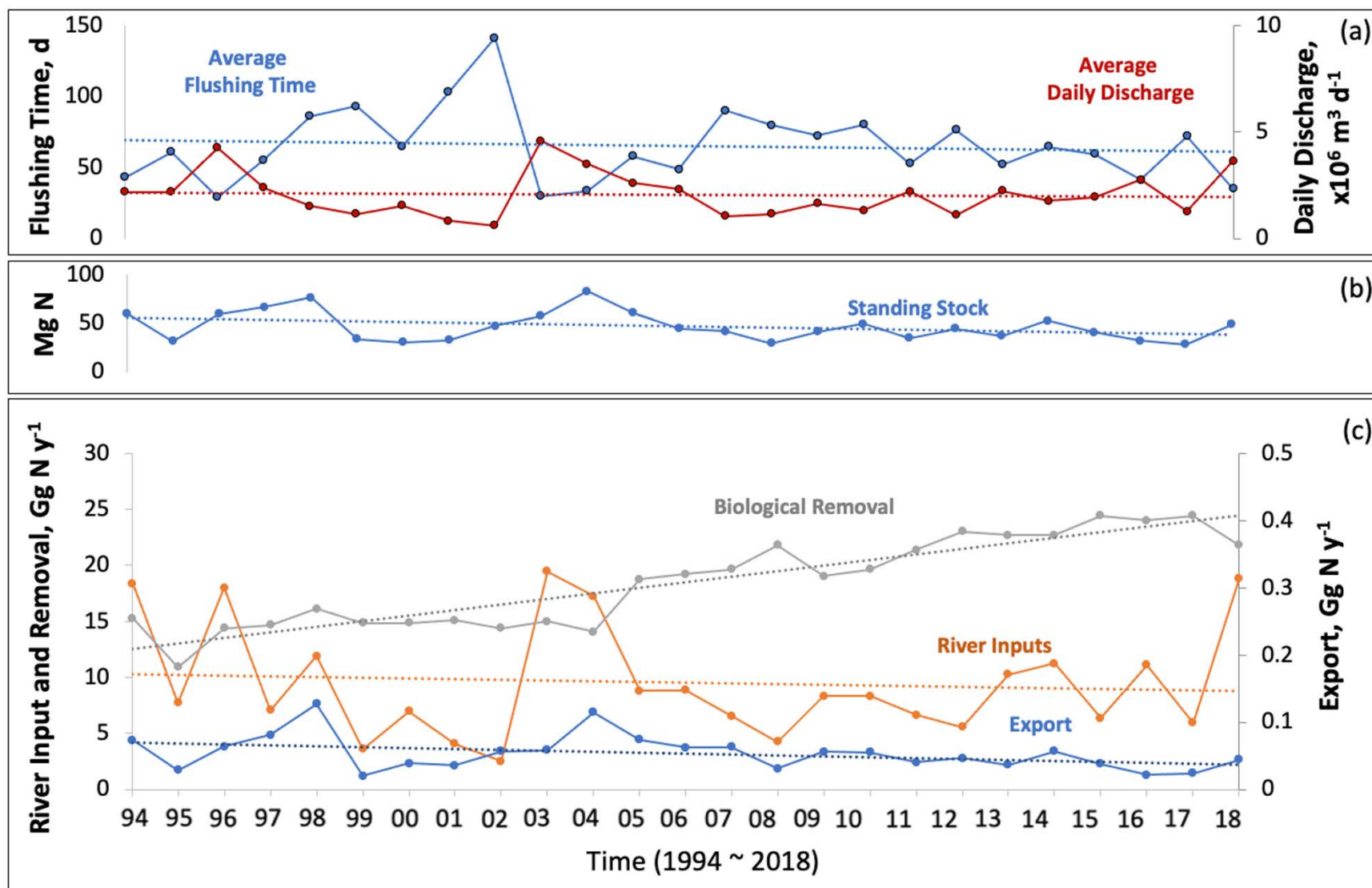
Figure 6. (a) Flushing time and daily discharge, (b) standing stock of DIN, and (c) computed DIN fluxes for the entire YRE. Linear regression equations for DIN standing stock ($y = -0.71x + 1471$; $r^2 = 0.12$), river inputs ($y = -0.064x + 137$; $r^2 = 0.01$), biological removal ($y = 0.50x - 983$; $r2 = 0.85$), and export ($y = -0.001x + 2.8$; $r^2 = 0.15$) as a function of year were all highly significant ($p < 0.0001$).
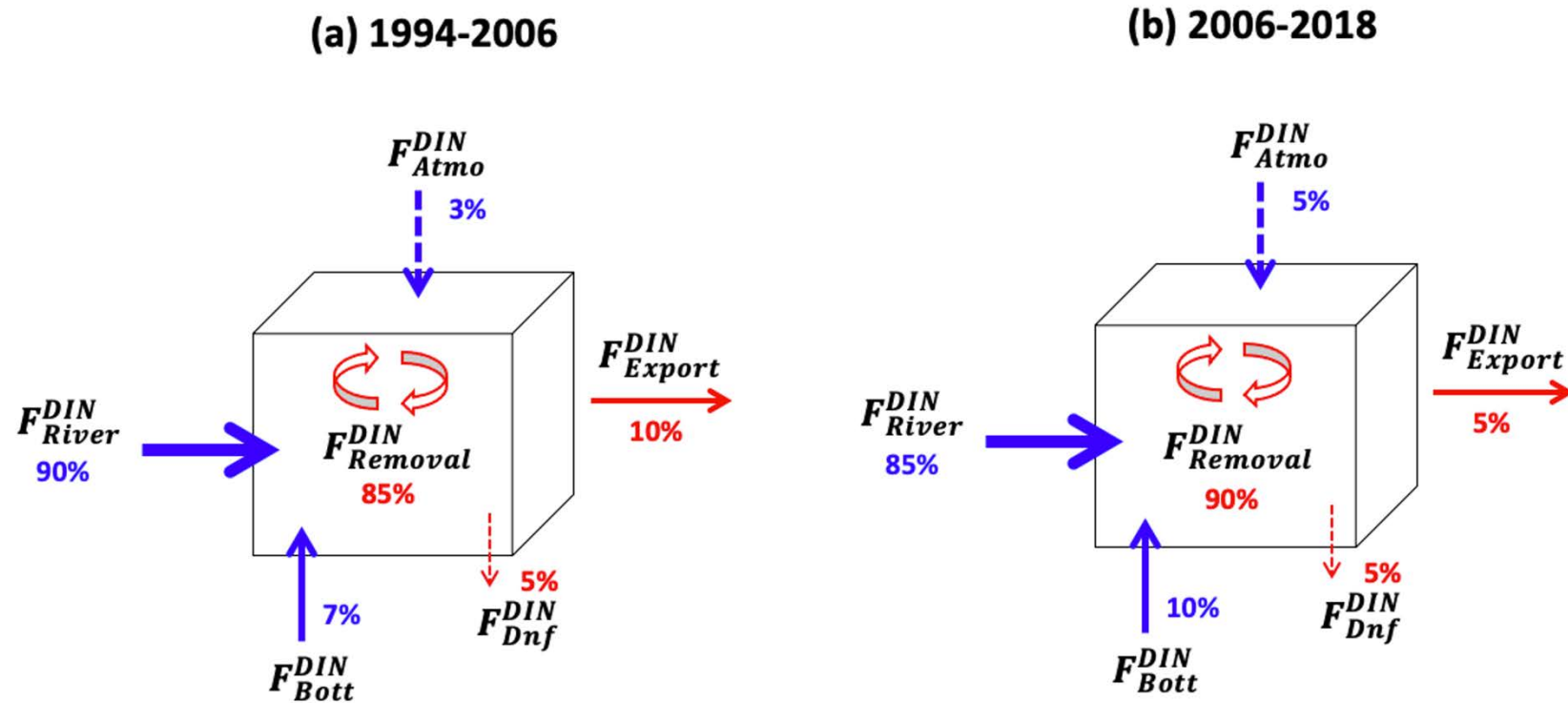
Figure 7. Annual DIN budgets for the YRE from the mass balance model, (a) averaged over the period 1994 to 2006 and (b) 2006 to 2018. Values are expressed as the percent contribution to total inputs (blue terms) and total outputs (red terms).
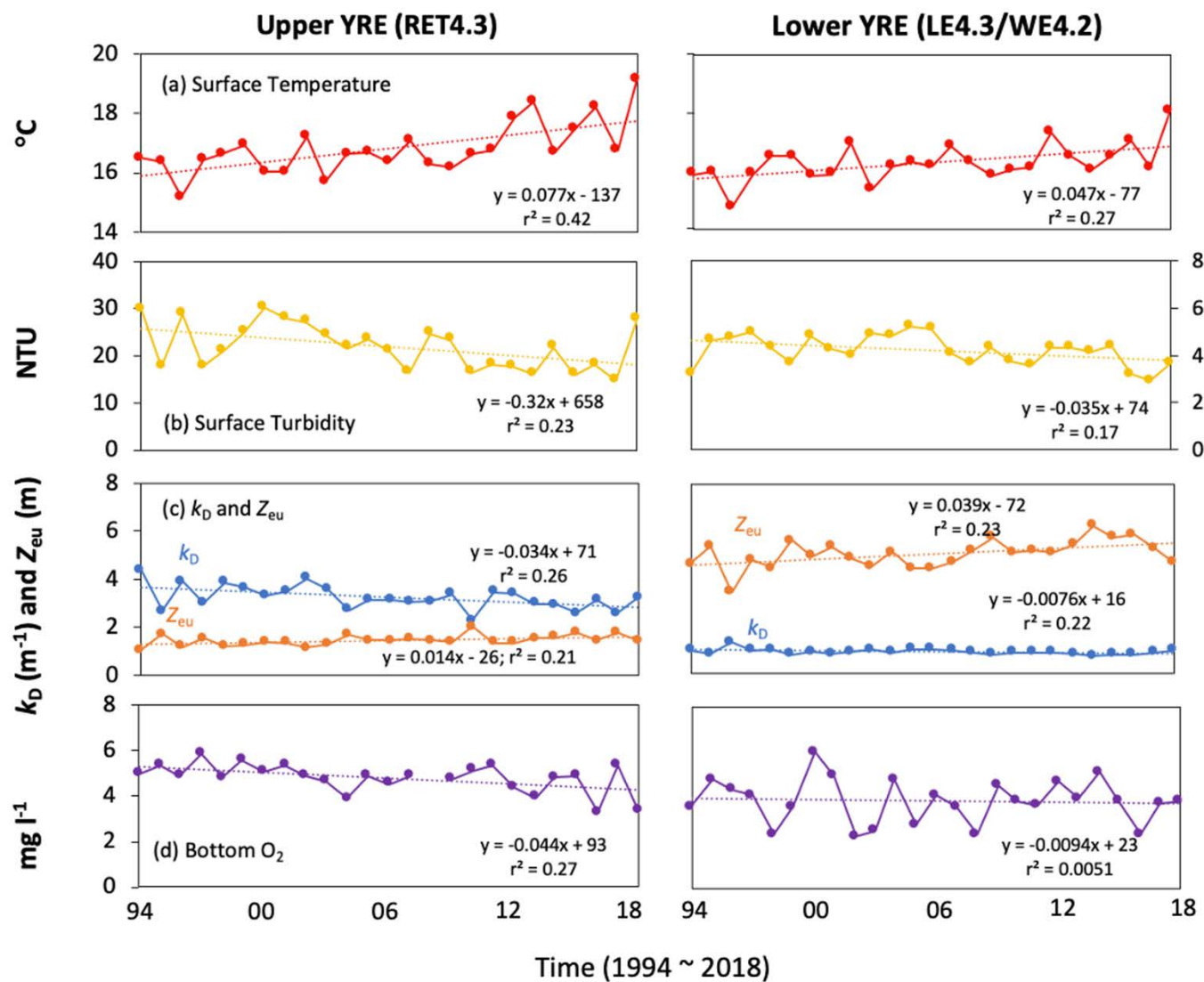
Figure 8. Time series of annual average (a) surface water temperature, (b) surface turbidity, (c) vertical attenuation coefficient (k_D) and euphotic depth (Z_{eu}), and (d) bottom oxygen concentration (averaged below the pycnocline) from CBP monitoring stations in the upper and lower YRE, respectively (see Fig. 1).

List of Tables

Table 1. Definitions and sources of data used in the N-mass balance model of the YRE.

Table 1. Definitions and sources of data used in the N-mass balance model of the YRE.

Unit	Definitions	Source
A (m^2)	Area of each box	Lake and Brush (2015a)
C_{River}^{DIN} (mmol m^{-3})	DIN concentrations in Pamunkey and Mattaponi Rivers	CBP
V_S (m^3)	Water volume of each box	Lake and Brush (2015a)
C_{EX}^{DIN} (mmol m^{-3})	Concentration gradient between adjacent boxes $C_{EX} = (C_{upper} - C_{lower})$ for DIN	Computed
λ_{Flush} (d^{-1})	Flushing rate (reciprocal of flushing time)	Lake and Brush (2015a)
F_{River} (m^3 d^{-1})	River discharge	USGS
F_{River}^{DIN} (mol d^{-1})	DIN input from riverine discharge	USGS, CBP
F_{Atmo}^{DIN} (mol d^{-1})	DIN input from atmospheric deposition	0.3 mmol N m^{-2} d^{-1} Kemp et al. (2005); Lake and Brush (2015a)
F_{Bott}^{DIN} (mol d^{-1})	Net benthic efflux of DIN from bottom sediments	1.2 mmol N m^{-2} d^{-1} Cowan and Boynton (1996); Boynton and Bailey (2008)
F_{Dnf}^{DIN} (mol d^{-1})	Denitrification rate	78-108 μmol m^{-2} h^{-1} Kana et al. (2006)
F_{Export}^{DIN} (mol d^{-1})	Export to the Chesapeake Bay from the YRE	Computed
$F_{Removal}^{DIN}$ (mol d^{-1})	Removal by phytoplankton uptake	Computed